Multiple-collision model for high-energy nucleus-nucleus collisions

Cheuk-Yin Wong
Oak Ridge National Laboratory, Oak Ridge, Tennessee 37831

Zhong-Dao Lu
Oak Ridge National Laboratory, Oak Ridge, Tennessee 37831
and Institute of Atomic Energy, Academia Sinica, Beijing, China
(Received 20 May 1988; revised manuscript received 16 January 1989)

We use a Glauber multiple-collision model to examine the dynamics of nucleus-nucleus collisions. The model introduces a stopping law which describes how a baryon loses energy in a basic baryon-baryon collision and a particle production law which relates the distribution of produced particles to the baryon momentum loss. The model gives results which compare well with the recent WA80 experimental data of ^{16}O on various targets at 60 and 200 GeV per projectile nucleon and reveals a high degree of stopping in these high-energy nuclear collisions.

I. INTRODUCTION

Recently, there has been much interest in relativistic heavy-ion collisions, which stems from the possibility of creating matter with very high energy densities.[1-14] The energy densities may be high enough to exceed the critical energy density required for a phase transition from the ordinary confined hadronic matter to the unconfined quark-gluon plasma. Experimental searches and identification of the quark-gluon plasma may provide new insight into the question of quark confinement. Furthermore, the creation of the domain of high energy density may allow one to study matter under unusual conditions such as those which exist in the history of the early Universe. Initial experimental data have been obtained recently with relativistic heavy ions at CERN[5-12] and at Brookhaven.[13,14]

The study of the dynamics of a nucleus-nucleus collision has not yet reached a stage where such a process can be described from first principles, starting with the theory of QCD. There are many phenomenological models which attempt to describe the interaction processes. All of these models assume a multiple-collision process such as in the Glauber model.[15] All of these models assume that, as a first approximation, production of the nonleading particles occurs after the two nuclei have passed through each other, due to the requirement that the collided hadrons must be separated by a minimum distance before particle production can take place.[16-18] The models differ in their assumptions as to how the particles share their energies and where the sources of particle production are.

In the Lund model for heavy-ion collisions,[19,20] it is assumed that for low-p_T phenomena, the hadrons are not transversely excited but are only longitudinally stretched. The hadrons undergoing interaction exchange forward and backward light-cone momenta $E+p_z$ and $E-p_z$ during the collision. The excited hadrons subsequently decay after collisions have been completed and are the sources of particle production. The decay of these stretched hadrons is analyzed in the same way as in the decay of a stretched q-$\bar{q}$ pair which has been previously worked out in the older version of the Lund model for nucleon-nucleon and e^+-e^- collisions.[20]

In the dual parton model developed by Capella, Tran Thanh Van, and their collaborators[21] and other workers,[22] each hadron is considered to consist of elementary constituents whose momentum distributions inside the hadrons are inferred from other empirical considerations such as the dual resonance model. In a collision of these two hadrons, these constituents fragment into the detected particles according to certain assumed semiempirical fragmentation functions. For hadron- and nucleus-nucleus collisions, there are additional assumptions about the sea quarks which take up the momentum of the incident partons.

In the multiple-chain model proposed by Kinoshita, Minaka, and Sumiyoshi,[23-25] incident baryons make collisions with many nucleons in the target nucleus. Each collision leads to the formation of a chain which later evolves into produced particles. After each collision, each chain also acquires a momentum. Each chain decays into hadrons, depending on a fragmentation function which can be different for different chains. A Monte Carlo program for pA collisions using such a model has been developed recently.[25]

Besides these models, there is also the valon model developed by Hwa and his collaborators which treats nucleus-nucleus collisions completely at the quark level.[26] The basic ingredients are the structure functions, the fragmentation functions, and the recombination functions, which need to be parametrized by comparison with experimental data.

Following the spirit of the dual parton model and the multichain model, we seek a *simple* Glauber-type multiple-collision model which brings out the essential features of the physics involved and is flexible enough to allow the extraction of useful information on the nature of nuclear stopping and particle production in nucleus-nucleus collisions. The physics of the process can, of

course, be described at the quark level as in the dual parton model or the valon model. In fact, there are many processes (such as in the peripheral direct fragmentation of a single constituent quark that has suffered no collision) which can only be described in terms of constituent quarks. However, there are many other aspects of the collision processes for which a *collective* description of the basic units in terms of baryons will suffice. Clearly, the slowing down of the baryon matter and the production of particles in a complicated multiple-collision process will not be sensitive to whether one uses a microscopic or a "collective" description of the collision process, because the basic physics involves the loss of the energy baryon matter and the consideration of energy conservation for particle production. At high energies, the velocities of all the particles are close to the speed of light; quarks which belong to the same nucleon will likely be found near the same spatial vicinity after the collision. Thus, a collection of collisions at the quark-quark level can be described in terms of equivalent collisions at the baryon-baryon level. For this reason, we shall use baryons as the basic unit of collision. This "collective" description has the advantage of simplicity and economy of effort. We know that multiple collisions of the incident baryon matter do take place, as evidenced by the loss of the longitudinal momentum of a nucleon when it passes through a nucleus.[27,28] This momentum loss depends on the thickness of the target nucleus. In each collision, the baryon number is conserved. We shall loosely associate these leading baryon-content-carrying objects as "baryons." It is reasonable to assume that the leading hadrons (leading baryons in this case) are the ones which can undergo multiple collisions. After each collision, a strong field is created between the colliding objects, and the leading baryons are the sources of the strong fields. While the strong field in each collision later stretches out longitudinally and hadronizes into produced particles (such as pions), the leading particles can proceed forward and make other collisions. As they are the sources of the strong field between the colliding baryons after each collision, their longitudinal momentum must be dissipated in each collision. If we follow the sequence of multiple collisions of one such baryon (Fig. 1), the collisions it suffers occur sequentially, and the different collisions are separated by a timelike space-time interval. By causality, the momentum of the product baryon after one baryon-baryon collision should be related to the momentum of the baryon before the collision by a causal relation. We shall describe the longitudinal-momentum loss of these baryons by a "stopping law" which expresses the degree of inelasticity of the collision in a causal daughter-parent relation. Along with the loss of longitudinal energy of the baryons, particles are later produced (represented schematically by the wavy lines in Fig. 1). We can take the shape of the rapidity distribution of the produced particles to be governed in a way similar to that in nucleon-nucleon collisions. In this way, the physics of the longitudinal energy loss and particle production can enter into the dynamics of heavy-ion collisions directly and shows up in the spectrum of the particles detected in high-energy heavy-ion reactions. In fact, it was previously found that[29–34] if we analyzed high-energy nucleon-nucleus collisions in terms of the Glauber model, qualitative agreement with the particle production and nuclear stopping data could be obtained when we ascribed to each nucleon-nucleon collision approximately the same characteristics as it has in free space.

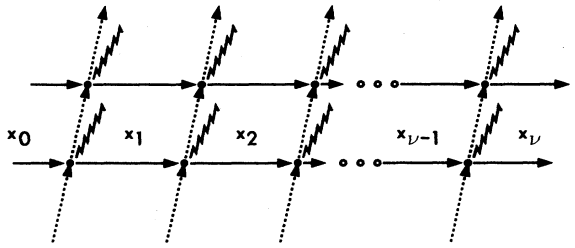

FIG. 1. Schematic representation of the multiple-collision process. Here, the solid line represents the projectile nucleons and the dashed lines represent the target nucleons. In each collision, the nucleons lose energy momentum which later leads to the production of particles represented by the wavy lines. The light-cone variable after the νth collision is represented by x_ν. We assume that the light-cone variable x_ν is related to $x_{\nu-1}$ by a causal relationship.

There are also other similar applications of the multiple-collision model to high-energy nuclear collisions. Ludlam and others[35,36] assume that in each collision, the energy loss and the spectrum of produced particles are taken to be the same as calculated with the ISAJET program which has been written to reproduce the nucleon-nucleon collision data,[37] while the leading clusters can continue on to make more collisions as they pass through the other nucleus. Results from such an approach are in qualitative agreement with hadron-nucleus collision data.

This paper is organized as follows. In Sec. II, we discuss the characteristics of a nucleon-nucleon collision which are of special interest in the study of nucleus-nucleus collisions. The shape of the rapidity distribution of the produced particles and the momentum distribution of nucleons in a nucleon-nucleon collision are used to form the parametrization that is used later on. In Sec. III, we discuss the Glauber model of nucleus-nucleus collisions and introduce the stopping law and the procedures for the evaluation of the spectrum of the produced particles. The results are shown in Sec. IV, and are then compared with the WA80 experimental data.[5–7] In Sec. V we examine the implications of the present calculation.

II. NUCLEON-NUCLEON COLLISIONS

Nucleon-nucleon collisions provide basic data relevant to nucleus-nucleus collisions. The nucleon-nucleon inelastic cross section is approximately 32 mb which is relatively energy independent[38] when the collision energy is much greater than the particle production threshold. About 6% of this can be attributed to diffractive dissociation for which the leading particle loses very little energy. Thus, for our discussion of particle production and stopping of baryons, two nucleons undergoing elastic or

diffractive dissociation collisions can be considered as suffering essentially no collision at all. On this basis, we shall consider only nondiffractive inelastic collisions and shall mean by a nucleon-nucleon collision to be a nondiffractive inelastic nucleon-nucleon collision with a cross section σ_{in} of 29.4 mb.

In a nucleon-nucleon or a baryon-baryon inelastic collision, there should be at least two baryons among the product hadrons because of the law of baryon conservation. The degree of inelasticity can be measured by the forward light-cone variables x_+ for the projectile and x_- for the target baryon. More specifically, in the reaction $a+b\to c+X$, with b the beam particle, a the target particle, and c the detected particle, the light-cone variable for projectile fragmentation x_+ is defined as

$$x_+=\frac{c_0+c_z}{b_0+b_z}\ , \tag{2.1}$$

and the light-cone variable for target fragmentation x_- is defined as

$$x_-=\frac{c_0-c_z}{a_0-a_z}\ . \tag{2.2}$$

In Eqs. (2.1) and (2.2), we have used the particle symbol also to represent the four-momentum of that particle.

To study the degree of energy loss of a projectile in an inelastic collision, we examine the shape of the distribution $d\sigma/dx$ as a function of the (forward) light-cone variable x. (For simplicity of notation, we shall omit the subscript + in the forward light-cone variable when we discuss the inelastic projectile-baryon distribution.) Except for the diffractive dissociation region in the vicinity of $x\sim 1$, the differential cross section is nearly flat. (See Fig. 1 of Ref. 30.) If one extrapolates to small regions of x and does not include diffractive dissociation in their consideration, an approximate representation of the (differential) cross section is

$$\frac{d\sigma}{dx}\approx\frac{\sigma_{\text{in}}}{1-x_L}\theta(1-x)\theta(x-x_L)\ , \tag{2.3}$$

where x_L is the lower limit of x as required by energy and momentum consideration.[30]

The loss of the baryon energy is associated with the production of particles. Experimental data of nucleon-nucleon collisions reveal that about 90% of the produced particles are pions; the rest consists of kaons, baryons, antibaryons and other particles. Their average transverse momentum is about 350 MeV/c which increases slightly at very high energies.[39] The total multiplicity of particles increases with the c.m. energy approximately in a logarithmic way. The rapidity distribution is in the form of a bell-shaped curve for $\sqrt{s}\sim 10$ GeV, but at the CERN ISR energies[40] with $\sqrt{s}$ up to 63 GeV, the rapidity distribution dN/dy of the produced charged particles assumes the shape of a plateau having a value of about 2 in the central rapidity region.

In the $p+p\to\pi^{\pm}+X$ reaction, the momentum distribution of the produced pions is usually represented in terms of light-cone variables $x_{\pm}$ which specifies the light-cone momentum fraction of the detected pion relative to the light-cone momentum of the parent particle. Experimental measurements in the projectile-fragmentation region give a pion invariant cross section (which is proportional to dN/dy) of the form $(1-x_+)^a$ with the value of $a\sim 3$–4 (Refs. 38 and 40). By symmetry, there must be a similar distribution for the pions produced in the target fragmentation region. We can make this distribution symmetric with respect to the two regions by parametrizing the rapidity distribution of the produced pions in the form

$$\frac{dN}{dy}(y)=A\left[(1-x_+)(1-x_-)\right]^a\ . \tag{2.4}$$

This rapidity distribution can be written entirely in terms of the rapidity variable y by expressing x_+ in terms of y as

$$x_+=\frac{m_{\pi T}}{M_N}\exp(y-y_B) \tag{2.5}$$

and x_- in terms of y as

$$x_-=\frac{m_{\pi T}}{m_N}\exp(y_T-y)\ . \tag{2.6}$$

In Eqs. (2.5) and (2.6), y_B and y_T are the rapidities of the beam nucleon and target nucleon, respectively, m_N is the mass of a nucleon, and $m_{\pi T}$ is the transverse mass of a pion given by

$$m_{\pi T}=(m_\pi^2+B_T^2)^{1/2}\ , \tag{2.7}$$

where m_π is the mass of a pion and B_T is the average transverse momentum $\langle p_T\rangle$ of the produced particles. In this form, in the projectile-fragmentation region, as y is close to y_B, we have $x_+\sim 1$ and $x_-\sim 0$ and consequently, the distribution exhibits a $(1-x_+)^a$ behavior. Similarly, for the target-fragmentation region, the distribution varies as $(1-x_-)^a$. In terms of the rapidity variable, the rapidity distribution assumes a bell-shaped distribution at low energies and a plateau-shaped distribution as the energy increases. We find that the following set of parameters gives a satisfactory description of the experimental rapidity distribution of nonleading charged particles:

$$\begin{aligned} A&=0.75+0.38\ln\sqrt{s}\ ,\\ a&=3.5+0.7\ln\sqrt{s}\ , \end{aligned} \tag{2.8}$$

and

$$B_T=0.27+0.037\ln\sqrt{s}\ ,$$

where B_T is in units of GeV/c and $\sqrt{s}$ in units of GeV.

III. GLAUBER MODEL OF NUCLEUS-NUCLEUS COLLISIONS

The Glauber multiple-collision model for the collision of composite particles is based on the concept of a mean free path with the assumption of a basic constituent "parton-parton" cross section. In the naive quark model

of a hadron, the partons are just the valence quarks. In a nucleus, one can again describe a nucleus as a collection of quarks and gluons. A simpler and a more "collective" description, which may be valid for many purposes, is to treat the nucleons as the partons. When a parton of one particle passes through the other particle, it may become excited and may, in principle have a different cross section. We can understand much of the geometrical concepts of the collision process if we take the basic parton-parton cross section $\sigma_{\rm in}$ to be the same throughout the passage of the parton in the other particle.

We consider the collision of composite particles B and A. Given a density distribution of nucleons $\rho_B(r)$ and $\rho_A(r)$, the positions of the B and A nucleons in the nuclei in their respective rest frames can be randomly picked from a random-number generator. This type of a Monte Carlo sampling procedure will be used repeatedly in our calculation; it is useful to outline briefly the steps involved. When we are given a probability distribution $f(z)$ such that the probability of the occurrence of z in the interval between z and $z+dz$ is

$$dP=f(z)dz \ , \tag{3.1}$$

we construct (either numerically or analytically) the integral

$$P(z)=\int_{x_L}^{z} f(z')dz' \ , \tag{3.2}$$

where z_L is the lower limit of z. Clearly, $P(z)$ is a monotonically increasing function of z; it equals zero at the lower limit of z and equals unity at the upper limit of z. We then pick a random number P_0 in the interval between 0 and 1, and obtain the value z_0 at which $P(z_0)=P_0$ by an interpolation. The occurrence of the random number P_0 then signals the occurrence of z_0. A set of randomly distributed P_0 values will give a set of z_0 distributed according to $f(z)$.

To describe the dynamics of the colliding nucleons, we shall boost the coordinate system from the laboratory frame to the nucleon-nucleon center-of-mass frame in which a nucleon in the projectile has a momentum $m_N\beta\gamma$ that is equal and opposite to the momentum $-m_N\beta\gamma$ of a nucleon in the target. In this frame, the longitudinal coordinates of the projectile and the target nucleons are contracted by a factor of γ. We start the calculation at the moment when the longitudinal separation of the two nuclei is 4 fm greater than the sum of their Lorentz-contracted radii $(R_A+R_B)/\gamma$ where $R_i=1.2A_i^{1/3}$ fm.

We can sample the impact parameter b using the Glauber model[15] for which the inelastic cross section is given by[30–32]

$$\sigma_{\rm in}^{AB}=\int d\mathbf{b}\{1-[1-\sigma_{\rm in}T_{AB}(\mathbf{b})]^{AB}\} \ , \tag{3.3}$$

where $T_{AB}(\mathbf{b})$ is the thickness function defined by

$$T_{AB}(\mathbf{b})=\int d\mathbf{b}_A dz_A d\mathbf{b}_B dz_B \rho_A(\mathbf{b}_A,z_A)\rho_B(\mathbf{b}_B,z_B) \times\delta(\mathbf{b}-\mathbf{b}_A+\mathbf{b}_B) \ . \tag{3.4}$$

with $T_{AB}(\mathbf{b})$, $\rho_A(\mathbf{r}_A)$, and $\rho_B(\mathbf{r}_b)$ normalized according to

$$\int T_{AB}(\mathbf{b})d\mathbf{b}=\int d\mathbf{r}_A\rho_A(\mathbf{r}_A)=\int d\mathbf{r}_B\rho_B(\mathbf{r}_B)=1 \ . \tag{3.5}$$

Consequently, the probability distribution for the impact parameter $\mathbf{b}$ is

$$\frac{dP(\mathbf{b})}{d\mathbf{b}}=\frac{1-[1-\sigma_{\rm in}T_{AB}(\mathbf{b})]^{AB}}{\sigma_{\rm in}^{AB}} \ . \tag{3.6}$$

This probability distribution allows us to select an impact parameter b by a Monte Carlo sampling. After this selection, the longitudinal and the transverse coordinates of all the nucleons can be determined from their initial coordinates. We can now use the baryon-baryon inelastic cross section to decompose the nucleus-nucleus collisions in terms of a collection of tubes of colliding nucleons. Starting with a nucleon in the projectile B, all of the projectile and target nucleons which lie within a transverse radial distance of $(\sigma_{\rm in}/\pi)^{1/2}$ form a tube in which all of the projectile nucleons within that tube collide with all of the target nucleons in the tube. Out of the remaining nucleons, another projectile nucleon is then picked to form another tube of projectile nucleons and target nucleons with a tube cross section of $\sigma_{\rm in}$. As the trajectories of the colliding baryons are nearly straight, it is a good approximation to neglect the exchange of nucleons from one tube to another during the collision process. Then, a nucleus-nucleus collision is decomposed into a collection of tubes i with $i=1,i_{\max}$. In the ith tube, N_i projectile nucleons collide with M_i target nucleons in an essentially one-dimensional manner.

We shall describe the longitudinal-momentum loss of the colliding baryons by a "stopping law" which expresses the degree of longitudinal inelasticity of the collision. The stopping law is simplest in terms of the light-cone variable x. Following Kinoshita, Minaka, and Sumiyoshi,[23] we choose to write the stopping law as

$$P(x)=\frac{\alpha}{1-x_L}\left[\frac{x-x_L}{1-x_L}\right]^{\alpha-1}\theta(1-x)\theta(x-x_L) \ , \tag{3.7}$$

where x is the light-cone variable or the longitudinal-momentum fraction of the "daughter" baryon b' after a baryon-baryon collision relative to the "parent" baryon b before the collision as defined previously in Eq. (2.1):

$$x=\frac{b_0'+b_z'}{b_0+b_z} \ , \tag{3.8}$$

and x_L is the minimum light-cone variable for the "daughter" baryon. We shall assume that the scattered projectile baryon picks up forward light-cone momentum only while the scattered target baryon picks up backward light-cone momentum. Then, the minimum value x_L corresponds to the rapidity of the center of mass of the colliding baryons. A flat distribution, such as observed in nucleon-nucleon collisions in free space, [Eq. (2.8)], corresponds to $\alpha=1$. The greater the value of α, the less the degree of baryon stopping in its passage through a nucleus.

For numerical purposes, we need to describe the collision of many particles. It is more convenient to work in the rapidity space and to give a rapidity coordinate y_i to

each particle. Then, the above stopping law can be transformed into a stopping law in terms of the rapidity variables: For a collision of two baryons with rapidity variables y_1 and y_2, the probability distribution of finding the baryon with rapidity y_1' after collision is[41]

$$W(y_1';y_1,y_2)=\frac{\alpha e^{y_1'}}{e^{y_1}-e^{y_L}}\left[\frac{e^{y_1'}-e^{y_L}}{e^{y_1}-e^{y_L}}\right]^{\alpha-1}\theta(y_1-y_1')\times\theta(y_1'-y_L)\ , \tag{3.9}$$

where y_L is the rapidity of the center of mass of the colliding system. This stopping law gives the rapidity y_1' of baryon 1 after the collision by a Monte Carlo sampling. The rapidity of the other baryon y_2' is obtained in a similar manner.

In order to obtain the momenta of all particles in each event, we need the transverse distribution of the scattered baryons. We parametrized it as in nucleon-nucleon collisions using the experimental $p+p\rightarrow p+X$ data:[42]

$$F_b(p_t)=\begin{cases}\mathcal{N}\exp(-cp_t^2) & \text{if } 0\le p_t\le 0.9 \text{ GeV},\\ \mathcal{N}'\exp(-c'p_t) & \text{if } 0.9 \text{ GeV}\le p_t\le 3 \text{ GeV},\end{cases} \tag{3.10}$$

where $\mathcal{N}'/\mathcal{N}=2.53$, $c=3.3$ GeV^{-2}, and $c'=4.0$ GeV^{-1}.

Knowing the rapidity variables of the baryons before and after the collision, we can now get the produced particle spectra in the center-of-mass frame (of the two colliding baryons) taken to obey a distribution of the form

$$\frac{d^3N}{dy\,d\mathbf{p}_T}=C\{[x_+(\max)-x_+][x_-(\max)-x_-]\}^{\alpha-1}\times f_\pi(p_T)\ , \tag{3.11}$$

where the light-cone variables x_+ and x_- are defined in terms of the rapidities of the produced particles as before [Eqs. (2.5) and (2.6)] while $x_+(\max)$ and $x_-(\max)$ are the maximum light-cone momentum fractions of the produced particles which are determined by the rapidities of the scattered baryons:

$$x_+(\max)=1-x_+(\text{scattered projectile nucleon})\ , \tag{3.12}$$

and

$$x_-(\max)=1-x_-(\text{scattered target nucleon})\ . \tag{3.13}$$

We have included in Eq. (3.11) a transverse- momentum distribution of the produced particles. It is parametrized by using the experimental $p+p\rightarrow\pi+X$ data[43] in the form

$$f_\pi(p_t)=\begin{cases}\mathcal{N}\exp(-cp_t) & \text{if } 0\le p_t\le 0.9 \text{ GeV}\ ,\\ \mathcal{N}'\exp(-c'p_t) & \text{if } 0.9\text{GeV}\le p_t\le 3 \text{ GeV}\ ,\end{cases} \tag{3.14}$$

where $\mathcal{N}'/\mathcal{N}=0.341$, $c=6.0$ GeV^{-1}, and $c'=4.8$ GeV^{-1}. The parameter a of Eq. (3.11) in the exponent $(a-1)$ is a function of the center-of-mass energy $\sqrt{s}$ of th two colliding baryons and is taken to be the same as that for the nucleon-nucleon collision [Eq. (2.8)] so that the folding of Eq. (3.11) with the momentum distributions [Eq. (2.3)] of the scattered baryons will give the momentum distribution of the produced particles [Eq. (2.4)] for a nucleon-nucleon collision. The constant C is a normalization constant.

The space-time dynamics of the nucleus-nucleus collision then follows from these simple laws. The colliding nucleons have coordinates specified by the initial conditions. In the nucleon-nucleon frame in which we work, the projectile nucleons have initial rapidity $(y_B-y_T)/2$ and the target nucleons have initial rapidity $-(y_B-y_T)/2$ where y_B and y_T are, respectively, the rapidity of the projectile and target nuclei in the laboratory frame.

With this initial specification, the nucleons are allowed to proceed forward in time until a collision among the N_i+M_i baryons takes place and the new resultant rapidities and transverse momenta of the two colliding baryons are then determined from the distribution Eqs. (3.9) and (3.10) with a random-number generator. The spectra of produced particles (which emerge later) are then calculated. The history of the baryons is then followed to the next collision and on and on, as in Fig. 1 of Ref. 41. A collision will be considered purely elastic without any change of rapidities if the center-of-mass energy of the colliding baryons is less than $\sqrt{s}\le 2.14$ GeV. We follow the dynamics until the time coordinate reaches 4 times the time it takes for a freely propagating baryon to traverse the sum of the diameter of the two nuclei. By this time, all of the projectile nucleons will have collided with all of the target nucleons. The energies and the momenta of the baryons, as well as the produced particles, are then collected into histogram bins. The same procedure is then repeated for the other tubes. This gives the spectra of the baryons and produced particles for one impact parameter. Another impact parameter is then selected according to the distribution of Eq. (3.6) until a sufficient number of collision cases are sampled to give the calculated results shown in the next section.

IV. RESULTS OF THE CALCULATIONS

A computer program MARCO was written to carry out the calculations mentioned in the last section. The nucleon densities of ^{12}C and ^{16}O are taken to be Gaussian distributions with root-mean-square radii of 2.53 and 2.75 fm, respectively.[44] For the heavier nuclei, we take the density to be a Woods-Saxon shape with a half-density radius given by[44]

$$R=(1.18A^{1/3}-0.48)\text{ fm}\ , \tag{4.1}$$

and a diffusivity $a=0.523$ fm. The baryon-baryon inelastic collision cross section is taken to be $\sigma_{\text{in}}=29.4$ mb (see Sec. 2.1).

In each calculation, a stopping-power index value α is assumed. After the spectra of the baryons and the produced particles are calculated, we make the appropriate kinematic cuts in order to compare the calculated results with the WA80 experimental data.[5–7] Specifically, in the

WA80 experiments, the measurement of the energy E_{ZDC} with the zero-degree calorimeter (ZDC) comes from particles falling within the pseudorapidity range of $\eta \geq 6.0$ and the measurement of the total transverse energy E_T with the midrapidity calorimeter (MIRAC) comes from particles with a pseudorapidity variable within the range of $2.4 \leq \eta \leq 5.5$. To signal the occurrence of an inelastic event, counting commences when the incident heavy ion suffers a substantial loss of the energy. In the WA80 experiments, events are triggered when the total energy in the zero-degree calorimeter E_{ZDC} is less than or equal to 88% of the incident heavy-ion energy, measured in the laboratory system.

Experimental measurements of various quantities have been obtained for oxygen beams at an incident energy of 60 and 200 GeV (per projectile nucleon), in reactions with the C, Cu, Ag, and Au targets.[5–12] For simplicity of notation, when we mention an incident energy, we shall often understand it to mean the incident energy per projectile nucleon. We shall focus our attention on the E_{ZDC} and E_T measurements of the WA80 Collaboration. We show in Figs. 2–7 the results calculated with the MARCO program and their comparison with the experimental

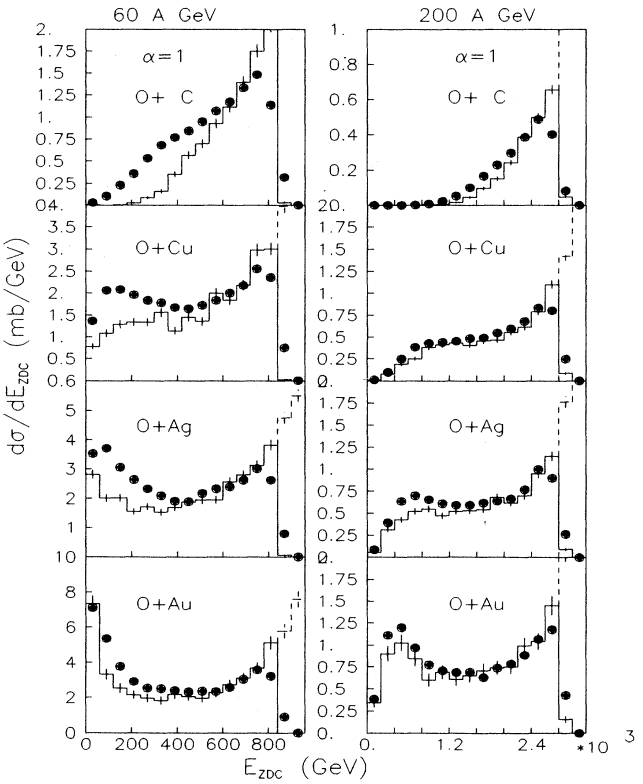

FIG. 2. Comparison of the zero-degree spectra obtained from the present model with $\alpha=1$ and the WA80 experimental data for the collision of ^{16}O at 60 and 200 GeV per nucleon. The experimental data are shown as solid circular points. The solid histogram shows the theoretical results with the trigger condition while the dashed histogram shows the theoretical results without the trigger condition.

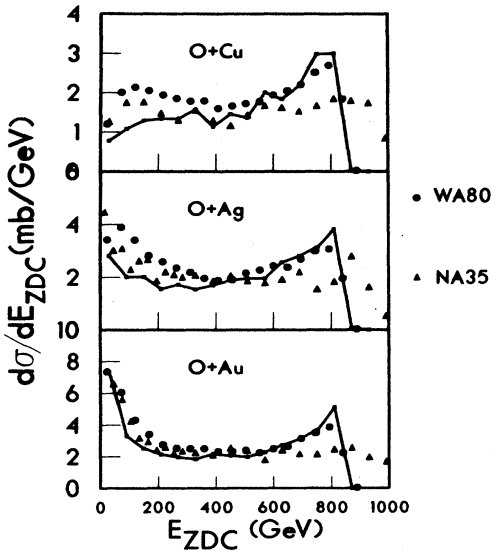

FIG. 3. Comparison of the zero-degree spectra obtained from the present model for $\alpha=1$ with the WA80 experimental data and the NA35 experimental data, for the collision of ^{16}O at 60 GeV per nucleon. The WA80 experimental data are represented by solid circular points while the NA35 data points are represented by triangles. The results from the present calculations are given by the solid line.

WA80 data. In these figures, the solid curves are the theoretical results, taking into account the trigger condition of the E_{ZDC} mentioned above. The results shown in the dashed curves do not take into account the trigger condition. The experimental data points are shown as

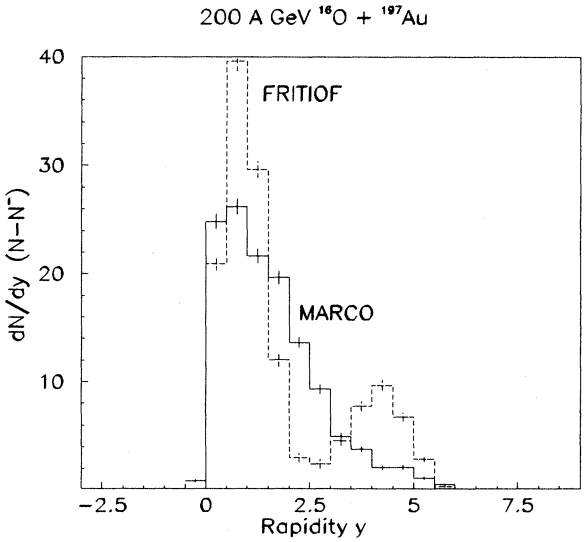

FIG. 4. The rapidity distribution of nucleons minus the rapidity distribution for the antinucleons for the collision of $^{16}O+^{197}Au$ at 200 GeV per nucleon and $b \leq 0.1$ fm. The solid histogram gives the results from the MARCO program while the dashed histogram gives the results from the FRITIOF program.

solid points in Figs. 2 and 5–7. Only the solid curves should be compared with experimental data.

In Fig. 2, the stopping power index α is set equal to 1, and we compare the results for the differential cross section $d\sigma/dE_{\mathrm{ZDC}}$ as measured by the energy E_{ZDC} deposited in the zero-degree calorimeter. One observes that the calculated results with the incorporation of the trigger condition agree quite well with the experimental data for the 200-GeV case. The agreement is not as good for the 60 GeV (per projectile nucleon) case, especially for the lighter target nuclei. It appears that for the 60-GeV case, there is more stopping of the projectile nucleons as indicated from the experimental data than is indicated by the theoretical calculations. However, on closer examination and comparison with the NA35 data[9] in Fig. 3, one finds that there may be some experimental uncertainties in the E_{ZDC} spectra for the lighter target nuclei at 60 GeV per projectile nucleon which need further experimental investigations. In the NA35 experiments, there is a so-called "veto" counter which has the same geometrical acceptance and function as the WA80 zero-degree calorimeter. Thus, the quantity E_{ZDC} of the WA80 experiment is approximately equivalent to E_{veto} of the NA35 experiment. Events are triggered by a different condition on an upstream scintillator counter which affects only the spectra at the high E_{ZDC} end. Thus, when we compare the experimental WA80 and NA35 data, we should not compare the high-E_{ZDC} end of the spectra directly. The NA35 group presented results for the E_{veto} spectra in the collision of ^{16}O on Cu, Ag, and Au at 60 GeV and on Au at 200 GeV (per projectile nucleon). One finds that the data of O+Au at the incident energy of 60 GeV per projectile nucleon from the two groups agree very well (except at the large values of E_{ZDC} due to different trigger conditions to cut off the spectra at large values of E_{ZDC}). For the collision of O on Au at 200 GeV per projectile nucleon, the WA80 peak at 0.4 GeV is shifted slightly to 0.2 GeV and the other parts of the spectra are slightly lower. But on the whole, the two measurements are quite similar. However, for O on Cu and O on Ag at 60 GeV per projectile nucleon, the spectra for small values of E_{ZDC} (up to 300 GeV) from the two measurements are different. In this region of small E_{ZDC} the calculated spectra (the solid curves in Fig. 3) also agree better with the NA35 spectra than they do with the WA80 spectra, for O on Cu at 60 GeV per projectile nucleon. It is clear that there are some experimental uncertainties concerning the spectra at small values of E_{ZDC} for the 60-GeV

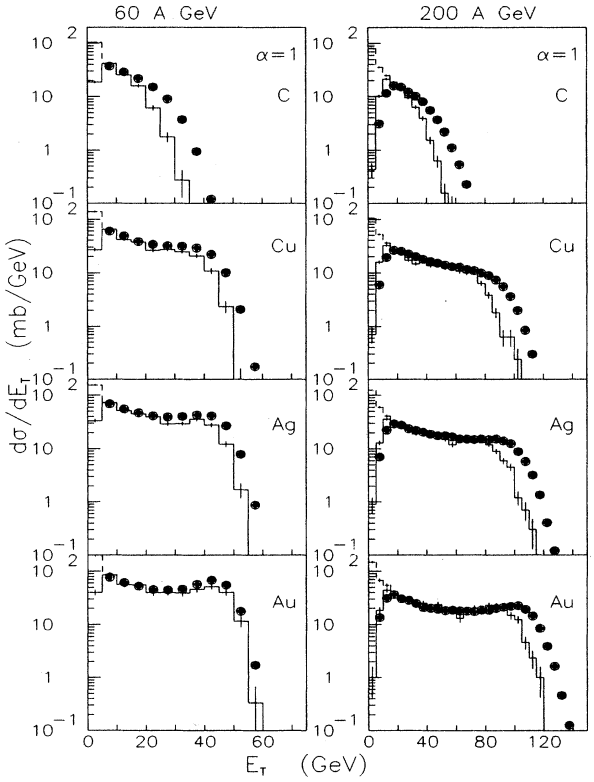

FIG. 5. Comparison of the transverse-energy spectra obtained from the present model with $\alpha=1$ and the WA80 experimental data. The data points are given as solid circular points. The solid histogram shows the theoretical results with the trigger condition while the dashed histogram shows the theoretical results without the trigger condition.

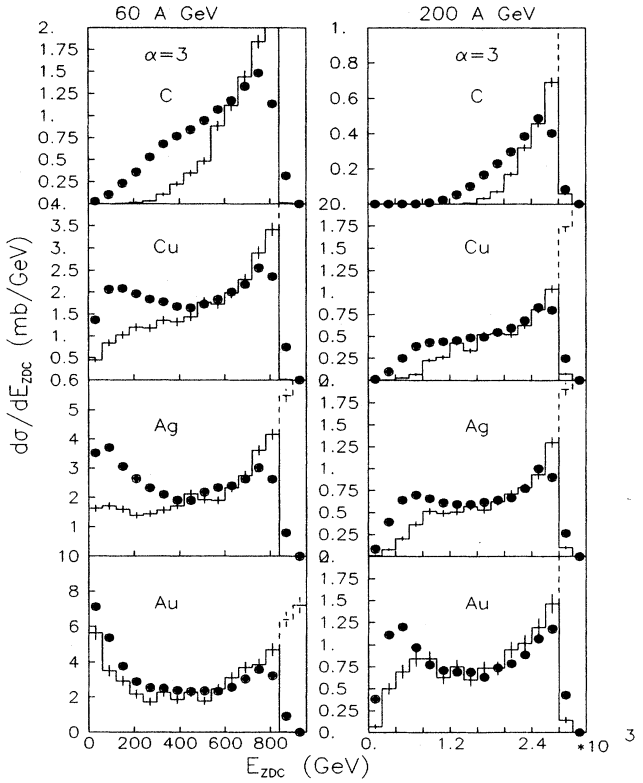

FIG. 6. Comparison of the zero-degree energy spectra obtained from the present model with $\alpha=3$ and the WA80 data. The experimental data are given as solid circular points. The solid histogram shows the theoretical results with the trigger condition while the dashed histogram shows the theoretical results without the trigger condition.

case which need experimental studies.

We compare our $d\sigma/dE_{\mathrm{ZDC}}$ results with those of the FRITIOF program of the Lund model where theoretical results were presented[5,7] corresponding to two different sets of geometrical parameters. We find that the theoretical results $d\sigma/dE_{\mathrm{ZDC}}$ obtained by FRITIOF are similar to those obtained here. Thus, the two models give similar results for the *total* energy in the zero-degree spectrometer. However, there are finer differences in the rapidity distribution of the baryons after the collision. We show in Fig. 4 the rapidity distribution of the nucleons minus the rapidity distribution of the antinucleons for an impact parameter $b \leq 0.1$ fm. The present MARCO program gives a one-peaked rapidity distribution which is a monotonically decreasing function of rapidity for $y > 1$. On the other hand, the FRITIOF program gives a two-peaked distribution of the scattered baryon matter:[45] one peak for the projectile scattered baryon matter and another peak for the scattered target baryon matter. There is a dip in the central rapidity region. A measurement of the baryon rapidity distribution for central collisions may help distinguish the two different models. In such a measurement, there are additional contributions of the baryons from nucleon-antinucleon pair production which has a peak in the central rapidity region. When this is taken into account, the dip in the central rapidity region is still very prominent in the FRITIOF calculation.

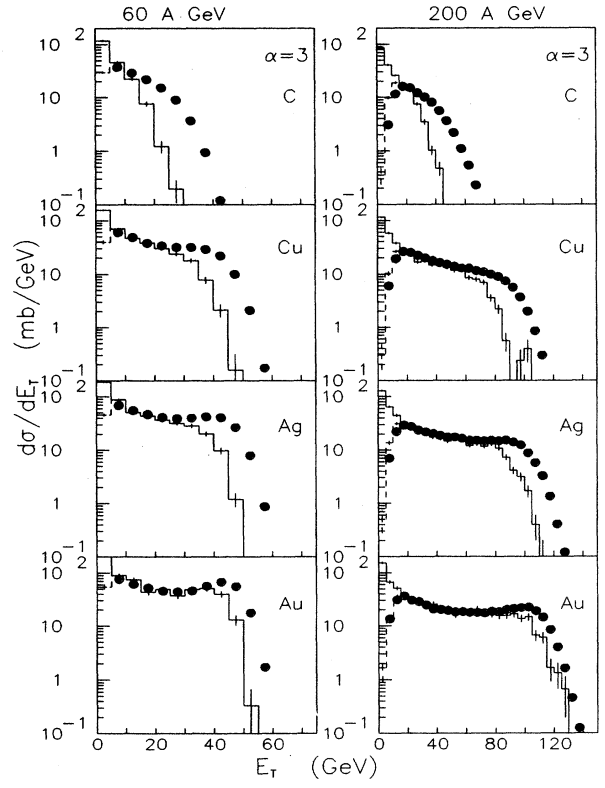

FIG. 7. Comparison of the transverse-energy spectra obtained from the present model with $\alpha=3$ and WA80 data. The experimental data are given as solid circular points. The solid histogram shows the theoretical results with the trigger condition while the dashed histogram shows the theoretical results without the trigger condition.

In Fig. 5 we show the transverse energy E_T spectra measured in the MIRAC detector and the E_T spectra calculated with the present model using $\alpha=1$. The calculated $d\sigma/dE_T$ results give reasonable agreement with the experimental data. There are, however, deviations from the high-E_T region for the case of 200 GeV per nucleon. The experimental differential cross sections $d\sigma/dE_T$ at large values of the transverse energy are greater than their corresponding calculated differential cross sections. On the other hand, the calculated E_T spectra are very sensitive to the value of the lower limit of the kinematic cut of the pseudorapidity variable η assumed. A change of the lower limit $\eta=2.4$ to $\eta=2.2$ will increase the maximum value of E_T (at which $d\sigma/dE_T$ drops down rapidly) by about 10%. Upon comparison of the transverse-energy spectra of Fig. 4 obtained in the present calculation with the theoretical results of FRITIOF in Ref. 7, we find again that the two models give results which are similar to each other. Both models predict maximum values of E_T which are smaller than the experimental maximum values of E_T.

The present model does not include the contributions to the transverse energy arising from the rescattering of the produced particles and of the recoiling target nucleon with the spectator target nucleons. There can be additional contributions to the transverse-energy spectrum from such collisions. This may be the reason why the experimental $d\sigma/dE_T$ extends to much larger values of E_T than those calculated here.

The longitudinal momentum of the recoiling target nucleons in the laboratory system increases as the incident energy increases. The secondary particles they generate concentrate at smaller angles, as the incident energy increases. Because the MIRAC detector subtends a maximum fixed angle of about 12°, it will accept more such secondary particles as the incident energy increases. This may explain why in the 200-GeV collision the experimental $d\sigma/dE_T$ extends proportionally farther out in E_T (as compared to the theoretical predictions) than in the 60-GeV collision.

Aside from these possible standard sources of transverse energy, one should be on the lookout for other possible sources of large transverse energies such as the formation of a quark-gluon plasma or the hydrodynamical expansion of a highly compressed mixed phase of quark-gluon plasma and hadron matter. In our calculations for central collisions, the spatial locations of the colliding baryons and their points of collisions are very close in longitudinal coordinates because of the Lorentz contraction. In consequence, the spatial densities of the baryon matter and the produced particle matter are high over a very small region of longitudinal space. This is very conducive for the formation of a quark-gluon plasma. Whatever is the matter that emerges in this small spatial region, it will be highly compressed. If the transverse size of this zone is large enough, local hydrodynamical equilibrium can be reached so that the longitudinal momen-

tum can be converted into the transverse momentum of the particles and an expansion in the transverse direction of the compressed matter (in addition to an expansion in the longitudinal direction) will take place and will lead to a larger value of the transverse energy.

To see how the zero-degree spectra and the transverse-energy spectra may be affected by the degree of nuclear stopping, we set α equal to 3 and obtain reuslts for the zero-degree spectra and the transverse-energy spectra shown in Figs. 6 and 7. We find from Fig. 6 that the $E_{\rm ZDC}$ spectra are sensitive to the stopping index α. The good agreement for the 200-GeV case which we obtained previously for $\alpha=1$ is no longer obtained. From Eq. (3.7), we see that the greater the value of α, the greater is the light-cone momentum retained by the baryons after a collision, and thus the smaller the ability of the nuclear matter to slow down the incident baryon matter. Indeed, the theoretical results for $\alpha=3$ give a cross section that is lower than the experimental $d\sigma/dE_{\rm ZDC}$ for small values of $E_{\rm ZDC}$ but larger than the experimental cross sections for larger values of $E_{\rm ZDC}$. In the transverse-energy data in Fig. 7, the deviations of the transverse energy at the high end of E_T become even more pronounced. A stopping law index of $\alpha=3$ does not give as good a description as $\alpha=1$.

V. CONCLUSIONS AND DISCUSSIONS

We have presented a simple multiple-collision model to describe the nucleus-nucleus collision process. The basic assumptions of the model are that multiple-collision processes occur and that the leading baryons are the objects which undergo multiple collisions. In each collision, the leading baryons leave behind sources for the strong field while the leading particles themselves proceed forward. The leading particles are different from the produced hadron matter which comes from the pair-creation mechanism arising from the strong field created between the two sources. We assume that the way the leading particles lose energy is related by a causal daughter-parent relation in each collision, and thus we ascribe a stopping law to specify the probability distribution of the momentum fraction lost in each collision. Particle production is assumed to be governed by another law in which the shape of the produced-particle spectrum in the rapidity space is the same as that in nucleon-nucleon collision in free space. In this description, the important factors are conveniently separated into a part which deals with stopping and a part which is concerned with particle production. We have assumed a simple stopping law and a particle production law for these processes. Other forms of the stopping law and the particle production law are also possible. It is clear that such a phenomenological theory requires for its implementation many confrontations of the theory with experimental data. The simplicity of model may bring out the important features of the collision process.

In our first analysis using a simple stopping law of the form $P(x)\sim\alpha x^{\alpha}$, it is found that in the WA80 experiments, the energy deposited in the zero-degree calorimeter and the transverse energy measured in the midrapidity calorimeter are approximately represented by the stopping-power index $\alpha=1$, which is also the stopping-power index for nucleon-nucleon collision in free space. This implies that the energy loss of the nucleons when they traverse another nucleus can be represented roughly as a successive multiple-collision process in which each collision loses energy approximately as in free space. As a phenomenological description, it may serve the purpose of comparing future data both to refine the model and to look for unexpected surprises.

The results obtained here also reveal the high degree of stopping the baryon matter suffers in high-energy nuclear collisions. The stopping-power index of $\alpha=1$ extracted here shows that approximately half of the forward light-cone momentum of the colliding baryon is lost in each collision. The greater the number of collisions, the greater will be the degree of stopping. Therefore, the baryon matter can be very effectively stopped in central collisions of very heavy nuclei. In the collision of a lead projectile nucleus on a lead target nucleus in a head-on collision, an area prescribed by a transverse distance of 4 fm has tube-tube collisions with more than five nucleons in each tube. It is therefore instructive to study the collision of a tube of five nucleons on another tube of five nucleons to obtain a rough idea of the magnitude of the energy density created in high-energy heavy-nuclei collisions. Previously, we estimated the energy density of the produced particles in the collision of a tube of five nucleons with another tube of five nucleons when the projectile nucleus has an incident energy of 15 GeV per projectile nucleon (energy measured in the laboratory system).[41] We can follow the method of Ref. 41 to consider the collision at the higher energies of 60 and 200 GeV per projectile nucleon. With a stopping index of $\alpha=1$ extracted here in the present work, we find that the baryons are essentially stopped in the center-of-mass system. It is therefore convenient to go to the center-of-mass system to find out the energy density of the produced matter. Because of the Lorentz contraction, the spatial locations of the baryons and their points of collision have only very small longitudinal extension. For example, in the 200-GeV-per-nucleon collision, numerical calculations show that the separation of the left- and the right-most collisions in the longitudinal direction is of the order of 0.7 fm in the 200-GeV collision, and about 0.9 fm in the 60-GeV collision. Thus, after the occurrence of the collisions, the emergence of the produced particles will be found in a small region of longitudinal space. We can again follow the method used in Ref. 41 to estimate the energy density at a time (for definiteness we take $t=3$ fm/c, for example) after the two tubes touch each other. The difference in the initial energy and the final energy of the baryons divided by the volume enclosed by the collision region gives the energy density of the produced particles. We can add an extension of 1 fm to both ends at the point of the furthermost collisions to take into account the streaming of the produced particles from the collision zone.[41] We then obtain an energy density of ~ 12 GeV for the 200-GeV-per-nucleon collision, and ~ 6 GeV for the 60-GeV-per-nucleon collision. These are very large energy densities. In addition, the baryon den-

sity is very compressed in this small region of space; it reaches a value of about 10 times the normal nuclear matter density in the 200-GeV collision and about 6 times normal nuclear matter density in the 60-GeV collision. Therefore, the energy density arising from the rest mass of the baryons is also very high. The total energy density is thus substantially higher than the threshold energy density of a few GeV/fm^3 for the occurrence of a quark-gluon plasma.[1] By way of comparison, at the lower energy of 15 GeV per nucleon (in the laboratory system), we have estimated an energy density of 2–3 GeV/fm^3 which might result in the bombardment of a tube of five nucleons on a tube of five nucleons.[41] The large increase in the energy density for the more energetic collisions arises because of the conversion of a larger initial longitudinal energy to the energy of produced particles. The estimates given here show that it is a very promising experimental prospect to study high-energy nuclear collisions with an accelerator which can accelerate heavy projectiles such as Pb to about 100 GeV per projectile nucleon so as to explore the possible formation of a quark-gluon plasma with a high baryon content.

It should be pointed out that there are additional effects which need to be included in future, more refined calculations. After a time delay following a baryon-baryon collision, produced pions will materialize and will participate in secondary collisions with nucleons in the central-rapidity region. These collisions will slow down the baryons and contribute to a larger transverse energy. The collision of the target recoiling nucleons with the target spectator nucleons will also contribute to the transverse energy. These additional effects may explain the difference between the experimental transverse-energy spectrum and the calculated spectrum. As the baryons pile up together, there are additional effects due to the baryon equation of state which will lead to a repulsive mean field for the baryons and an outward explosion of baryons. If the quark-gluon plasma is formed during the course of the collision, the dynamics will follow a different course. The signature for the presence of the quark-gluon plasma is a subject worthy of future investigations.[1]

ACKNOWLEDGMENTS

The authors wish to thank Dr. T. Awes, Dr. F. Obenshain, and Dr. Soren Sorenson for stimulating discussions and encouragement. One of us (Z.D.L.) would like to thank Professor P. Siemens for financial support without which this work would not have been completed. He also wishes to thank the Nuclear Theory Group of Oak Ridge National Laboratory for its kind hospitality. This research was supported by the Division of Nuclear Physics, U.S. Department of Energy under Contract No. DE-AC05-840R21400 with Martin Marietta Energy Systems, Inc.

[1]For a review of current research, see *Quark Matter '87,* proceedings of the Sixth International Conference on Ultrarelativistic Nucleus-Nucleus Collisions, Munster, West Germany, 1987 [Z. Phys. C **38**, 1–370 (1988)]; *Proceedings of the Fifth International Conference on Ultrarelativistic Nucleus-Nucleus Collisions,* Pacific Grove, California, 1986, edited by L. S. Schroeder and M. Gyulassy [Nucl. Phys. **A461**, Nos. 1 and 2 (1987)]; *Quark Matter '84,* proceedings of the Fourth International Conference on Ultrarelativistic Nucleus-Nucleus Collisions, Helsinki, Finland, 1984, edited by K. Kajantie (Lecture Notes in Physics, Vol. 221) (Springer, Berlin, 1985); *Quark Matter '83,* proceedings of the Third International Conference on Ultrarelativistic Nucleus-Nucleus Collisions, Upton, New York, 1983, edited by T. W. Ludlam and H. E. Wegner [Nucl. Phys. **A418** (1984)]; L. McLerran, Rev. Mod. Phys. **58**, 1021 (1988).

[2]A. S. Goldhaber, Nature (London) **275**, 114 (1978); R. Anishetty, P. Koehler, and L. McLerran, Phys. Rev. D **22**, 2793 (1980); J. Kapusta, Phys. Rev. C **27**, 2037 (1983); W. Busza and A. S. Goldhaber, Phys. Lett. A **139**, 235 (1984); M. Gyulassy, Phys. Rev. D **30**, 961 (1984); C. Y. Wong, Phys. Rev. C **33**, 1340 (1986).

[3]J. D. Bjorken, Phys. Rev. D **27**, 140 (1983).

[4]C. Y. Wong, Phys. Rev. D **30**, 961 (1984).

[5]WA80 Collaboration, R. Albrecht *et al.*, Phys. Lett. B **199**, 297 (1987).

[6]WA80 Collaboration, R. Albrecht *et al.*, Phys. Lett. B **201**, 390 (1988); **202**, 596 (1988); WA80 Collaboration, H. Löhner *et al.*, Z. Phys. C **38**, 97 (1988).

[7]WA80 Collaboration, S. P. Sorensen *et al.*, Z. Phys. C **38**, 3 (1988).

[8]NA35 Collaboration, A. Bamberger *et al.*, Phys. Lett. B **184**, 271 (1987); NA35 Collaboration, A. Sandoval *et al.*, Nucl. Phys. **A461**, 465 (1987); NA35 Collaboration, A. Bamberger *et al.* (unpublished); NA35 Collaboration, H. Ströbele *et al.*, Z. Phys. C **38**, 89 (1988); NA35 Collaboration, T. Humanic *et al.*, *ibid.* **38**, 79 (1988); NA35 Collaboration, G. Vesztergombi *et al.*, *ibid.* **38**, 129 (1988).

[9]NA35 Collaboration, W. Heck *et al.*, Z. Phys. C **38**, 19 (1988).

[10]NA34 HELIOS Collaboration, T. Akesson *et al.*, Z. Phys. (to be published).

[11]NA38 Collaboration, A. Bussiere *et al.*, Z. Phys. C **38**, 133 (1988); NA38 Collaboration, P. Sonderegger *et al.*, *ibid.* **38**, 133 (1988).

[12]P. L. Jain, K. Sen Gupta, and G. Singh, Phys. Rev. Lett. **59**, 2531 (1987); G. Gerbier, W. Williams, P. B. Price, and R. Guoziao, *ibid.* **59**, 2535 (1987); EMU01 Collaboration, M. I. Adamovich *et al.*, Phys. Lett. B **201**, 397 (1988); EMU07 Collaboration, L. M. Barbier *et al.* (unpublished); I. Otterlund, Z. Phys. C **38**, 65 (1988).

[13]E802 Collaboration, T. Abbott *et al.*, Phys. Lett. B **197**, 285 (1987); E802 Collaboration, Y. Miake *et al.*, Z. Phys. C **38**, 135 (1988).

[14]E814 Collaboration, B. Bassalleck *et al.* (unpublished).

[15]R. J. Glauber, in *Lectures in Theoretical Physics,* edited by W. E. Brittin and L. G. Dunham (Interscience, New York, 1959), Vol. 1, p. 315.

[16]J. Schwinger, Phys. Rev. **82**, 664 (1951); E. Brezin and C.

Ityzkson, Phys. Rev. D **2**, 1191 (1970).
[17]A. Casher, J. Kogut, and L. Susskind, Phys. Rev. D **10**, 732 (1974); A. Casher, H. Neuberger, and S. Nussinov, *ibid.* **20**, 179 (1979); H. Neuberger, *ibid.* **20**, 2936 (1979); C. B. Chiu and S. Nussinov, *ibid.* **20**, 945 (1979); I. K. Affleck *et al.*, Nucl. Phys. **B197**, 509 (1982).
[18]Ren-Chuan Wang and C. Y. Wong, Phys. Rev. D **38**, 348 (1988).
[19]B. Andersson, G. Gustafson, and B. Nilsson-Almqvist, Nucl. Phys. **B281**, 289 (1987); B. Nilsson-Almqvist and E. Stenlund, Comput. Phys. Commun. **43**, 387 (1987); M. Gyulassy, ATTILA, CERN Report No. TH.4794/87 (unpublished).
[20]A comprehensive review of the Lund model for nucleon-nucleon and e^+-e^- collisions can be found in B. Andersson, G. Gustafson, G. Ingelman, and T. Sjostrand, Phys. Rep. **97**, 31 (1983); other references on the Lund model: T. Sjostrand, Comput. Phys. Commun. **39**, 347 (1986); B. Andersson *et al.*, Z. Phys. C **1**, 105 (1979); **20**, 317 (1983).
[21]A. Capella and A. Krzywicki, Phys. Rev. D **18**, 3357 (1978); A. Capella and J. Tran Thanh Van, Z. Phys. C **10**, 249 (1981); A. Capella, C. Pajares, and A. V. Ramallo, Nucl. Phys. **B241**, 75 (1984); A. Capella, A. Staar, and J. Tran Thanh Van, Phys. Rev. D **32** 2933 (1985); A. Capella *et al.*, Z. Phys. C **33**, 541 (1987).
[22]J. Ranft, Phys. Rev. D **37**, 1842 (1988); K. Werner, Z. Phys. C **38**, 193 (1988).
[23]K. Kinoshita, A. Minaka, and H. Sumiyoshi, Prog. Theor. Phys. **63**, 1268 (1980).
[24]S. Daté, M. Gyulassy, and H. Sumiyoshi, Phys. Rev. D **32**, 619 (1985).
[25]Y. Iga, R. Hamatsu, S. Yamazaki, and H. Sumiyoshi, Z. Phys. C **38**, 557 (1988).
[26]R. C. Hwa, Phys. Rev. Lett. **52**, 492 (1984); R. C. Hwa and M. S. Zahir, Phys. Rev. D **31**, 499 (1985).
[27]A. Barton *et al.*, Phys. Rev. D **27**, 2580 (1983).
[28]W. Busza and A. S. Goldhaber, Phys. Lett. A **139**, 235 (1984).
[29]C. Y. Wong, Phys. Rev. Lett. **52**, 1393 (1984).
[30]C. Y. Wong, Phys. Rev. D **30**, 972 (1984).
[31]C. Y. Wong, Phys. Rev. D **30**, 961 (1984).
[32]C. Y. Wong, Phys. Rev. D **32**, 94 (1985).
[33]Sa Ban-Hao and C. Y. Wong, Phys. Rev. D **32**, 1706 (1985).
[34]C. Y. Wong, in *Medium Energy Physics,* proceedings of the International Symposium, Beijing, China, 1987, edited by Chiang Huan-Ching and Zheng Lin-Sheng (World Scientific, Singapore, 1988), p. 241.
[35]T. W. Ludlam (unpublished); A. Shor and T. W. Ludlam (unpublished).
[36]S. Frankel and W. Frati, Phys. Lett. B **196**, 399 (1987).
[37]F. Paige and S. D. Protopopescu, Brookhaven National Report No. BNL-31987, 1982 (unpublished).
[38]A. E. Brenner *et al.*, Phys. Rev. D **26**, 1497 (1982).
[39]K. Alpgard *et al.*, Phys. Lett. **107B**, 310 (1981).
[40]W. Thomé *et al.*, Nucl. Phys. **B129**, 365 (1977).
[41]C. Y. Wong, Phys. Rev. C **33**, 1340 (1986).
[42]D. Antreasyan *et al.*, Phys. Rev. D **19**, 764 (1979).
[43]B. Alper *et al.*, Phys. Lett. **47B**, 75 (1973); B. Alper *et al.*, Nucl. Phys. **B87**, 19 (1975).
[44]H. R. Collard, L. R. B. Elton, and R. Hofstadter, *Nuclear Radii* (Springer, Berlin, 1967).
[45]The authors would like to thank Dr. S. Sorensen and Dr. T. Awes for providing the results of the FRITIOF calculation.